Partial Transformation of Imogolite by Decylphosphonic Acid Yields an Interface Active Composite Material

Tobias Lange, Thibault Charpentier, Frédéric Gobeaux, Sophie Charton, Fabienne Testard, Antoine Thill

Partial Transformation of Imogolite by Decylphosphonic Acid Yields an Interface Active Composite Material

Authors:

Tobias Lange[1,2], Thibault Charpentier[2], Frédéric Gobeaux[2], Sophie Charton[1], Fabienne Testard[2], Antoine Thill[2]

Affiliations:

[1] CEA, DEN, Research Department on Mining and Fuel Recycling Processes, SA2I, F-30207 Bagnols-sur-Cèze, France.

[2] NIMBE, CEA, CNRS, Université Paris-Saclay, CEA Saclay, 91191 Gif-sur-Yvette Cedex, France.

Corresponding Author's Email : antoine.thill@cea.fr

Abstract

The phosphonic acid moiety is commonly used as an anchoring group for the surface modification of imogolite. However, the impact of the reaction on its structure has never been clearly analyzed before. We study the reaction of imogolite and decylphosphonic acid by combining infrared spectroscopy, X-ray scattering, scanning electron microscopy, transmission electron microscopy and solid-state nuclear magnetic resonance spectroscopy. Instead of a surface functionalization, we observe the formation of a lamellar phase interconnected with imogolite bundles. Although we find no evidence for grafted imogolite tubes, we observe the expected dispersion characteristics and stabilization of water in toluene emulsions described in literature. Based on the surface chemistry of imogolite we propose an explanation for the observed reactivity and link the structural features of the obtained composite material to its dispersibility in toluene and its observed properties at the toluene-water interface.

Introduction

Surface modification is often a mandatory step to explore the properties and potential applications of inorganic nanoparticles. Different approaches and compounds were developed to meet the specific requirements in diverse domains (polymer reinforcement, nanophotonics, catalysis, batteries, nanomedicine, etc.).[1-3] However, the potential influence of the used agent on the resulting particle shape, size and integrity keeps the topic challenging.[4] This is especially relevant for the surface modification of delicate structures like the one of imogolite nanotubes.

Imogolite is a nanotubular clay, characterized by a diameter between 2 nm and 3 nm and a general formula unit $(OH)_3Al_2O_3Si(OH)$.[5] The tube wall consists of a single gibbsite-like sheet, which is linked to isolated silanol groups at the internal surface.[6] The gibbsite-like external surface is covered by Al_2(μ-OH)groups. Various approaches and compounds have been studied to modify it, e.g. catechol[7], phosphates[8-11], silane[12], pyrrole[13], and stearic acid[14]. However, most of the studies aim to graft octadecylphosphonic acid or other phosphonic acids onto imogolite.[14-22] Yamamoto et al. were the first to study the chemisorption of octadecylphosphonic acid (ODPA) on imogolite.[14-15] They concluded that ODPA adsorbs to the surface of imogolite. Park et al. modified imogolite with ODPA and tetradecylphosphonic acid (TDPA).[16] The product was dispersible in toluene and microscopy pictures showed regular patterns, which were attributed to homogenously grafted imogolite. Bac et al. studied the reaction between ODPA and germanium

imogolite.[19] They concluded a successful grafting, although they observed the formation of a lamellar product in XRD. Picot et al. used ODPA modified imogolite to stabilize oil in water Pickering emulsions.[20]

All studies demonstrate the reactivity between imogolite and the phosphonic acid moiety. However, the evidence for the presence of grafted phosphonic acid on intact dispersed imogolite is ambiguous. The IR results only reveal the reactivity, but not the identity of the resulting phase.[14-15, 17-22] XRD and SAXS identified changes in the organization of the product, but led to different interpretations.[16, 19-20] Finally, the investigations by microscopy do not have the required resolution to evidence isolated grafted nanotubes with clarity or lack complementary characterization.[16-18]

A possible alternative reaction path for imogolite is the formation of bulk aluminum phosphonates. It is already known for the intercalation of gibbsite and kaolinite with phenylphosphonic acid (PPA)[23], the modification of aluminum oxide by ODPA[24] and PPA[4], and the modification of germanium imogolite by ODPA.[19] Nonetheless, it was shown that choosing favorable conditions prevents the bulk phosphonate formation and enables grafting of alumina by octylphosphonic acid.[25]

To assess if an efficient surface modification of imogolite is achieved, a combination of structural and chemical characterizations is necessary. In the present study, we explore the fate of imogolite during the reaction with alkylphosphonic acid at ambient conditions. We combine Fourier Transform Infra-Red (FTIR) spectroscopy, Small Angle X-ray Scattering (SAXS), Scanning Electron Microscopy (SEM), Transmission Electron Microscopy (TEM) and multinuclear Magic-Angle Spinning Nuclear Magnetic Resonance (MAS NMR) to study the chemical and structural modifications of imogolite.

Materials and Methods

Synthesis of Imogolite

Imogolite was synthesized using an adapted protocol inspired from Farmer et al.[26] Tetraethoxysilane was introduced under stirring into a 2 mM solution of $AlCl_3$ until a Si/Al ratio of 0.55 was reached. Under vigorous stirring, a 0.1 M NaOH solution was then added at a rate of 8 mmol·min^{-1} until an OH/Al ratio of 2 was reached. The suspension was then transferred to an oven, where it was kept at 90 °C for 5 days. Ultrafiltration with a 10 kDa membrane (SpectrumLabs) was then used to concentrate the imogolite dispersion up to a final concentration of 10 g·L^{-1}. The concentrated dispersion was centrifuged for 1 hour at 10,000 rpm to remove any trace of gibbsite, and then dialyzed against MilliQ water until reaching a

residual conductivity of less than 2 $\mu S \cdot cm^{-1}$. The resulting transparent dispersion was stored in a plastic container. Chemicals were obtained from Sigma-Aldrich and used as received.

Modification of Imogolite

In order to study the surface modification of imogolite by decylphosphonic acid (DPA) we adapted the protocols described in literature.[11, 15-16, 19-20] The prepared samples are listed in Table 1. For samples A1-A4 and B, 10 mL of aqueous imogolite dispersion (5 $g \cdot L^{-1}$) were diluted with ethanol (CARLO ERBA Reagents, p.a.) under strong stirring. Decylphosphonic acid (DPA, Sigma-Aldrich, 97 %) was dissolved in ethanol and then added to the imogolite dispersion. The resulting mixture was stirred at room temperature and turned whitish during reaction. The dispersed precipitate was collected by centrifugation and washed by three dispersion – centrifugation steps in ethanol. The sediment was finally dried under ambient conditions. For sample A5, DPA was dissolved in an aqueous ethanol solution (66:34, v/v, EtOH:H_2O) before adjusting the pH with 0.1 $mol \cdot L^{-1}$ NaOH (Sigma-Aldrich). The remaining procedure is unchanged.

We typically stopped the reaction after one day (samples A1-A5) to characterize the product. In order to obtain a complete reaction, one sample was kept stirring for 18 days (sample B). Sample A2 is a repetition of sample A1, to check the results repeatability for a given set of preparation conditions. Samples A3 and A4 have a smaller P: Al ratio compared to sample A1. Sample A5 was prepared in order to observe the influence of the initial acidity.Table 1 summarizes the different experimental conditions.

Table 1: Summary of the investigated reaction conditions, giving the stirring time, the molar ratio between phosphorous and aluminum, the volumetric solvent ratio (ethanol : water), and the concentration in DPA for each sample.

Sample	Time, days	P : Al	Solvent ratio EtOH : H_2O	C_{PA}, $mmol \cdot L^{-1}$
A1	1	5	95 : 5	5
A2	1	5	95 : 5	5
A3	1	3	95 : 5	3
A4	1	1	90 : 10	1
A5*	1	5	62.5 : 37.5	5

B	18	5	95 : 5	5

*pH adjusted to 5

Fourier Transform Infrared Spectroscopy

FTIR Spectra were collected in transmission from 4000 cm^{-1} to 400 cm^{-1} with a resolution of 4 cm^{-1} (Vertex 70, Bruker). KBr pellets were prepared by compressing approximately 1 mg of sample dispersed in 100 mg of KBr.

Small Angle X-ray Scattering

SAXS was acquired at 1.542 Å under vacuum with a Xeuss 2.0 apparatus (Xenocs). The intensity is plotted against the scattering vector $q = 4\pi \cdot \sin(\theta) \cdot \lambda^{-1}$, with λ being the wavelength and 2θ the scattering angle. The displayed q range from 1.0 nm^{-1} to 16.0 nm^{-1} was attained with a single sample to detector distance. The latter was calibrated with tetradecanol and the detector count was normalized by direct beam measurements. Samples were sealed in glass capillaries (diameter 1.5 mm, wall thickness 0.1 mm, WJM-Glas). Standard procedures were applied to subtract background scattering and to normalize the intensities.[27] The lamellar repeat distances were calculated by the position of their 0*k*0 progression, using $d = 2 \cdot \pi \cdot q^{-1}$.

Magic Angle Spinning Nuclear Magnetic Resonance Spectroscopy

MAS NMR data have been collected on a Bruker Avance II 500WB spectrometer operating at a magnetic field of 11.72 T using ZrO_2 rotors (outer diameter 4 mm) and Bruker HX and HXY CPMAS probes at a spinning frequency of 12500 Hz.

^{27}Al (I=5/2) MAS NMR spectra were acquired using a short single-pulse excitation of 1 µs (tip angle ~10°, to ensure quantitativeness of the spectra because of the non-homogeneous excitation of all sites with respect to their quadrupolar interaction strength) and a recycle delay of 1 s. Two-dimensional Multiple Quantum MAS (MQMAS, the triple quantum transition was used) were acquired using the three-pulse Z-filter sequence.[28]

^{31}P (I=1/2) MAS NMR spectra were acquired using a presaturation $(90°\text{-tau})_{N=20}$ period followed by a recovery delay of 32 s to ensure quantitativeness of the spectra.

Additionally, $^{27}Al\{^{31}P\}$ Rotational Echo DOuble Resonance (REDOR) experiments were performed to investigate the Al-P spatial proximities.[29]

The data was processed using an in-house made code.[30]

Dispersion of modified Imogolite, Emulsification and Interface Experiments

The modified imogolite was dispersed in toluene (CARLO ERBA, 99.8 %) directly after the washing steps (dispersion – centrifugation), and without prior drying. Emulsions were formed by mixing the dispersed modified imogolite suspension at 0.5 $g \cdot L^{-1}$ with water in $50/50_{v/v}$ proportion. Droplets of water were deposited on the interface between water and the above mentioned dispersion. The emulsions were observed on an Olympus IX81 microscope. High purity water (18.2 MΩ·cm) was used to create emulsions and liquid-liquid interfaces.

Scanning Electron Microscopy

The morphology of imogolite after the reaction with DPA was observed by scanning electron microscopy. The dispersed product was deposited on a plasma cleaned Si surface and left to dry. Observations were conducted on a Hitachi SU-70 microscope operated at 5 kV.

(Cryo-)Transmission Electron Microscopy

The morphology of synthesized imogolite was observed with cryogenic transmission electron microscopy. A drop of the solution was deposited on a copper grid covered with a holey carbon film (Quantifoil R2/2) that was previously treated by a plasma glow discharge. Excess of liquid on the grid was blotted out with filter paper and the grid was quickly plunged in liquid ethane to form a thin vitreous ice film. The whole process was performed using a Vitrobot apparatus (FEI Company). Observations were conducted at low temperature (−180 °C) on a JEOL 2010 FEG microscope operated at 200 kV. Images were recorded with a Gatan camera. To observe the morphology of the product dispersed in toluene, the dispersion was deposited on the copper grids and left to dry. The same camera and microscope were used at ambient temperature.

Results and Discussion

Transformation of imogolite by decylphosphonic acid

Imogolite

Imogolite was synthesized according to the protocol described in Materials and Methods. Cryo-TEM observations of the obtained aqueous dispersion (Figure 1a) evidence imogolite tubes in coexistence with globular allophane and proto-imogolite. The typical presence of other objects than imogolite reflects in the dampened SAXS curve (Figure 1b) and is in agreement with literature data on imogolite SAXS patterns.[31-33] Fitting the obtained curve with the scattering pattern of a hollow cylinder gives an outer tube radius of 2.8 nm, which is a typical value for synthetic dispersed imogolite.

The reactivity between the suspended particles and DPA is studied for the protocol described in material and methods. The products are characterized by FTIR, SAXS, multinuclear MAS NMR and electron microscopy to investigate the evolution with the reaction process. To identify the occurring transformations, all the prepared samples are systematically compared to pristine imogolite.

FTIR

The FTIR spectrum of imogolite has three main contributions (Figure 2). First, the hydroxyl stretching (3510 cm^{-1}) and bending vibrations (1636 cm^{-1}) originating mainly from internal water.[34] Secondly, the Al-O vibrations at 692 cm^{-1}, 596 cm^{-1}, 564 cm^{-1}, 503 cm^{-1} and 426 cm^{-1}, which are characteristic for the imogolite local structure (Figure 2b).[5] Lastly, the doublet appearing at 988 cm^{-1}/941 cm^{-1}, which is related to the asymmetric stretching mode of the isolated SiO_4 tetrahedra and is typical for the tubular shape of imogolite.[6, 31, 35-37] After reaction with DPA, all the characteristic regions of imogolite are retrieved in the FTIR spectra of samples A1-A5. Only the SiO_4 doublet shifts for each of these samples to 994 cm^{-1}-992 cm^{-1} / 938 cm^{-1}-935 cm^{-1}. For sample B the SiO_4 doublet is not observable, the appearance of the characteristic Al-O region (426 to 692 cm^{-1}) changes, and both the intensity and shape of the hydroxyl bands are different.

The appearance of CH_2 and CH_3 vibrations between 2960 cm^{-1} and 2850 cm^{-1} and at 1471 cm^{-1} indicate the presence of alkyl chains in all samples (Figure 2c). Comparing the CH_2 stretching bands of the products to those of DPA reveals no shift for sample B, while a qualitative shift towards higher wavenumbers is observed for samples A1-A5. This shift of the vibration bands for samples A1-A5 indicates slightly less ordered chains than in sample B, for which a similar degree of order as in the all-trans DPA is evidenced.[38]

Furthermore, a shouldered peak appears at 1080 cm^{-1} for samples A1-A5. The shoulder turns into several sharp bands for sample B. This new contribution indicates the formation of P-O-Al bonds in all samples and therefore a successful reaction between imogolite and DPA. Interesting to note is the disappearance of the P=O signal of DPA at 1232 cm^{-1} after reaction. A possible explanation could be a tridentate binding mode in the formed product.[39-40]

Overall, the spectra of samples A1-A5 show a high content of imogolite and are in good agreement with the findings of Yamamoto et al. for the reaction of ODPA with imogolite, and Bac et al. for the reaction between ODPA and germanium imogolite.[14-15, 19]

The spectrum of sample B suggests a rather low amount of residual imogolite due to the modification of the typical hydroxyl, Al-O and Si-O bands. It compares well with the spectrum of ODPA-modified imogolite presented by Picot et al.[20] The presence of several sharp P-O-Al peaks was also evidenced for aluminum organophosphonates and might indicate the presence of such a phase.[41]

Although IR demonstrates that a reaction has occurred between imogolite and DPA, it does not provide sufficient information to assess the integrity of the nanotubes after the reaction.

SAXS

The x-ray scattering pattern of imogolite shows a broad peak at 2.76 nm^{-1}, which is typical of disordered aggregated bundles in the dry powder (Figure 3). Significant modifications occur after reaction with DPA. For samples A1-A5, three peaks at 2.26 nm^{-1}, 4.51 nm^{-1} and 6.71 nm^{-1} superimpose the scattering curve of imogolite. Additional peaks are present at higher q values but not clearly visible due to noise. The exact position of these reflections varies slightly with the reaction conditions. Sample B shows peaks at 2.11 nm^{-1}, 4.26 nm^{-1}, 6.35 nm^{-1}, 8.49 nm^{-1}, 9.31 nm^{-1}, 10.58 nm^{-1}, 12.73 nm^{-1}, 13.65 nm^{-1} and 14.80 nm^{-1}, while the contribution of imogolite is hardly noticeable. Excluding the peaks at 9.31 nm^{-1} and 13.65 nm^{-1}, all the peaks in sample B are consistent with the 0*k*0 progression of a lamellar phase. For samples A1 and A4, this is not so evident on the first glance, since the first peak of imogolite bundles seems to shift towards smaller q values. However, the resulting increase in d spacing is not consistent with a DPA grafted tube, since the difference to the radius of an imogolite tube is only 0.6 nm. For sample B, the lamellar peaks are shifted to smaller angles and the reflections are better defined. This effect is consistent with larger lamellar domains and a higher order of organization of the alkyl chain, as observed in IR. The inter-lamellar spacing is 2.8 nm for samples A1-A5 and 2.9 nm for sample B. It is close to the values reported for lamellar phases

obtained with other decylphosphonate metal oxide phases such as aluminium decylphosphate (3 nm), calcium decylphosphate (3.1 nm) and calcium hydroxyapatite modified by decylphosphate (3 nm).[42-44]

Bac et al. already observed the formation of a lamellar phase following the reaction between germanium imogolite and ODPA.[19] They observed a peak in XRD at 1.65 nm, which most probably represents the 0*3*0 peak of aluminum octadecylphosphonate with a corresponding lamellar repeat distance of 5.0 nm.

Picot et al. found peaks at approximately q = 1.3 nm^{-1}, 2.6 nm^{-1}, 3.9 nm^{-1} in SAXS and interpreted them as the *k*0 progression of a 2D hexagonal phase.[20] Calculating the distance for a lamellar 0*k*0 progression from their values yields 4.8 nm, which is in good agreement with aluminum octadecylphosphonate.

Direct comparison with the XRD data on the reaction between ODPA and imogolite of Park et al. is difficult, since the used wavelength is missing and the data is noisy.[16] Nonetheless, the authors present scanning tunneling microscopy pictures where they observe a pattern with a repeat distance of d=5.1 nm for ODPA and 4.7 nm for TDPA after reaction with imogolite. These distances correlate to the chain length of the used phosphonic acid, but the presence of imogolite tubes in the structure is not unambiguously proven.

The d spacings of all these compounds appear to increase linearly with the carbon number of the alkylphosphonic acid (Figure 4), which indicates that the length of the alkyl chain is the main factor influencing the thickness, regardless of the nature of the inorganic part. Even for short chain phosphonates, the trend holds true. The only deviation is observed with the microscopy data reported by Park et al. for TDPA. The variation in d spacing for the reported octadecylphosphonates could be associated to different crystal structures as reported for phenylphosphonates. For aluminum phenylphosphonate the structure indeed depends on the synthesis condition.[45]

From SAXS, we can conclude that the reaction of imogolite with alkylphosphonic acid yields a lamellar phase for all experimental conditions (Table 1) and that no evidence of grafted imogolite is observed.

MAS NMR

Although MAS NMR is a useful tool for the characterization of imogolite, no study of the reaction between imogolite and phosphonic acids has been reported so far.[46-48] Since no relevant differences were observed between the samples A1-A5, the NMR investigation was restricted to the unreacted imogolite (reference), sample A1 and sample B.

The obtained ^{31}P MAS NMR spectra (Figure 5a) show no remaining DPA at 31 ppm (Figure S2) for the different products. Sample A1 has a single broad peak from 0 ppm to 35 ppm, while sample B shows

pronounced peaks at 2 ppm, 9.5 ppm and 13.5 ppm. The broad peak in sample A1 evidences the formation of P-O-Al bonds with distributed chemical environments. The latter develops into a more ordered structure with prolonged reaction time, as observed for sample B.

Pristine imogolite has a single peak at 8 ppm in ^{27}Al MAS NMR (Figure 5b), which is assigned to octahedral coordinated aluminum and clearly confirms the imogolite local structure.[46-47] Three peaks are visible in the ^{27}Al MAS NMR spectra for samples A1 and B. The peak centers and the corresponding relative area were obtained by deconvolution of the ^{27}Al MAS NMR spectra (Figure S3). The signals of sample A1 are centered at −5 ppm (24%), 8 ppm (69 %) and 47 ppm (7 %). The peak at −5 ppm exhibits a noticeable broadness. For sample B the signals are located at −13 ppm (69 %), 8 ppm (28 %) and 46 ppm (3%).

By collecting ^{27}Al {^{31}P} REDOR curves (Figure 5c), the spatial proximity of P to Al atoms was probed. The Al REDOR signal at −5 ppm and 47 ppm in sample A1 rapidly increases with time suggesting that Al atoms are in close vicinity to P atoms. This is not the case for the slowly increasing signal at 8 ppm, indicating that this site is able to interact with phosphorous, but does not directly coordinate to it. For sample B the Al atoms resonating at −13 ppm are close to P atoms, while the 8 ppm peak is not coordinated by P. Low peak intensity made it impossible to collect the data for the signal at 46 ppm and turned the data for the 8 ppm peak noisy.

In ^{27}Al MQMAS NMR (Figure 6) imogolite shows a NMR shift distribution mainly due to quadrupolar interactions. The MQMAS experiments for samples A1 and B confirm the presence of three sites. For sample A1 the signal at 8 ppm has a similar NMR shift distribution as unmodified imogolite, while the two new peaks at −5 ppm and 47 ppm display mainly a distribution in the isotropic shift (see dashed lines in Figure 6). This distribution indicates a lower degree of crystallinity in the new environments. For sample B the signal at −13 ppm has a more pronounced quadrupolar distribution than the signal at −5 ppm in sample A1 and is therefore more crystalline.

All samples show a signal at 8 ppm, hinting on the presence of unreacted imogolite tubes. ^{29}Si MAS NMR also confirms the presence of unreacted imogolite (Figure S2b). Due to the vicinity of P and Al, the peaks at −5 ppm and −13 ppm can be assigned to AlO_6 octahedrons with P in their second coordination shell, and the peaks at 47 ppm and 46 ppm to Q^4(4P) AlO_4-tetrahedra.[49] Similar shifted signals were reported for AlO_4[41, 45] and AlO_6[50] coordination in aluminum phenylphosphonates. From this result and the previous characterization it can be concluded that sample B mainly consists of rather crystalline aluminum decylphosphonate. This is supported by the sharp peaks in the ^{31}P spectrum, which were identified as a sign for crystalline aluminum alkylphosphonate.[24-25, 51] Sample A1 still has a high content of imogolite and

the new octahedral Al environment is less well defined. Furthermore, the ^{31}P spectrum shows a broad peak, which was identified by Lassiaz et al. as an indicator for a successful grafting reaction on aluminum oxide.[25, 51] However, in the present case the unresolved ^{31}P peak could also reflect the distributed chemical environments in a not exclusively crystalline phosphonate.

SEM and TEM

SEM of sample A5 (Figure 7a, b) shows aggregates with zones of needle-shape and platelet-like morphologies. Both types of morphology are connected. These aggregates appear as dark domains in TEM (Figure 7c). In their periphery, assemblies of aggregated nanotubes are visible. In between the network of imogolite bundles, small domains are present. Depending on their orientation in space, the aggregates show a lamellar organization. We did not find any structures hinting on grafted imogolite, i.e. imogolite surrounded by a corona of DPA.

Degradation versus surface modification

The obtained results challenge the commonly used scheme of grafted imogolite, where the phosphonic acid reacts with OH groups on the external wall of imogolite and forms covalent bonds by condensation.[18-19, 21-22] IR, ^{31}P MAS NMR and ^{27}Al {^{31}P} REDOR experiments give evidence for the formation of P-O-Al bonds. However, the found chemical shift in ^{27}Al MAS NMR and the SAXS results are in favor of the formation of a lamellar aluminum decylphosphonate structure. SEM and TEM support these findings by showing a mixture of lamellar phase and imogolite tube bundles, interconnected with each other. Overall, the results do not support a grafting reaction of DPA on imogolite but give evidence for the formation of a composite material.

The basis for this reactivity is the surface chemistry of imogolite, which is similar to gibbsite. The tube wall is covered in bridging Al_2(μ-OH) groups that correspond to the crystal face of gibbsite, while the terminal points have Al-OH / Al-OH_2^+ groups, similar to the crystal edges of gibbsite. The difference between those two sites is their affinity to participate in adsorption. The single coordinated hydroxyls are active, while the bridging hydroxyls are inert for adsorption processes at low adsorbate concentrations.[52-53] For phosphate, gibbsite starts to form aluminum phosphate phases at acidic pH that deposit on the faces of gibbsite.[54] It was suggested that the complexation of the gibbsite edge is an intermediate in this process.[54-55] Based on the structural similarity of metal phosphates and phosphonates,[56] we presume a similar reactivity for the sorption process of phosphonic acid on imogolite as for phosphate on gibbsite. At the studied conditions DPA does not adsorb or react with the bridging Al_2(μ-OH) groups of imogolite. It mainly

complexes Al-OH and Al-OH_2^+ groups and degrades imogolite tubes by forming lamellar aluminum decylphosphonate. Since those groups are mainly present at the terminal points of the tubes, the degradation is slow and it explains the high amount of residual tubes evidenced for samples A1-A5.

Dispersion of modified Imogolite, Emulsification and Interface Experiments

In the majority of the published studies the dispersibility of modified imogolite was taken as a proof of concept for the successful surface modification of imogolite by phosphonic acid.[16, 19-21] Although our results give no hint for surface modified imogolite tubes, the DPA modified imogolite is dispersible in toluene. It gives an almost clear liquid, which is slightly scattering light. Mixing this dispersion with water stabilizes a water in oil emulsion (Figure 8a, b and Figure S4). In contrast, bare imogolite gives an oil in water emulsion, as was already observed for hexane.[20] With the composite material, the droplets do not coalesce and can undergo deformations. This is also observed at the macroscopic scale, where an interface between the dispersed composite material and water is able to stabilize large aqueous droplets against coalescence (Figure 8c). This very specific behavior is related to the DPA modified imogolite and cannot be obtained with the interface between toluene and a bare imogolite dispersion. The ability to stabilize develops with contact time between the two phases and is generally not instantaneously present. The droplets are stable up to one year (experimental time), but collapse if the toluene evaporates. Illumination of the sample unveils the otherwise almost invisible surface precipitate (Figure 8), that forms after the contact between the dispersion and water, but does not exist in the toluene dispersion itself. The stabilized droplets can also be moved on the interface (see SI). We retrieve characteristics of “liquid marbles” for an oil/water system. Liquid marbles are defined for air/liquid systems as stabilized liquid droplets covered with hydrophobic particles. Thanks to the nanoparticles, the droplets are able to maintain their shapes even after deformation by external forces.[58-60]

Up to now, the dispersibility of alkylphosphonic acid modified imogolite in organic solvents was explained by a successful grafting reaction, and the resulting grafted imogolite was sketched as a tube with a brush-like corona of grafting agent.[16-20] The difference in hydrophilicity between the internal and the external surfaces of such a grafted tube was used to explain the formation of Pickering emulsions by ODPA modified imogolite.[20] However, the structure of dried modified imogolite (Figure7) suggests that the mode of stabilization has to be different.

Presuming a similar structure in its dispersed state as in its dried state (Figure 7), the imogolite-lamellar phase network would exhibit zones where either hydrophobic (lamellar phase) or hydrophilic areas (residual imogolite) dominate. While the hydrophobic areas promote the dispersion in toluene, the hydrophilic areas and the nanostructuration of the composite material could be responsible for its surface activity at the toluene/water interface. Further investigations are needed to elucidate the real stabilization mechanism for this system, but are out of the scope of this study.

Conclusion

We characterized the reaction between imogolite and DPA by several complementary methods, in particular a complete NMR study. Instead of a grafting reaction, we found the partial transformation of imogolite into a lamellar aluminum phosphonate. The resulting composite material consists of interconnected imogolite tube bundles and lamellar phase. The specific nanostructure of this material enables the dispersion in organic solvent and gives rise to interfacial properties leading to the stabilization of water droplets in toluene. Our results demonstrate that DPA (or phosphonic acids in general) are not appropriate reagents to modify the surface of imogolite nanotubes. We believe that the observed process might give insights into an approach to create hierarchical structures with novel properties from colloidal particles under mild conditions.

Acknowledgements

We want to thank M. Moskura for her help with MAS NMR and P. Picot for the helpful discussions. FEGSEM & EDX instrumentation was facilitated by the Institut des Matériaux de Paris Centre (IMPC FR2482) and was funded by Sorbonne Université, CNRS and by the C'Nano projects of the Région Ile-de-France. (Cryo-) TEM observations were made thanks to “Investissements d’Avenir” LabEx PALM (ANR-10-LABX-0039-PALM). This work was financed by the Amont-Aval CEA program.

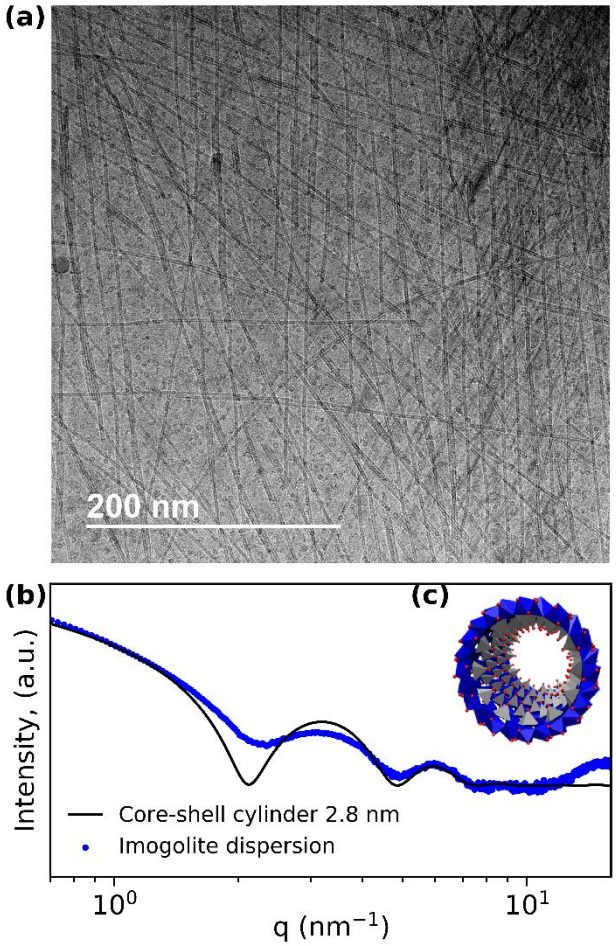

Figure 1. (a) Cryo-TEM picture of imogolite. Globular structures are allophane and proto-imogolite. (b) SAXS pattern of dispersed imogolite and a fit by a core-shell cylinder (see SI), yielding an outer diameter of 2.8 nm.(c) Inset of the imogolite structure, grey tetrahedra are centerd by silicon, blue octahedra are centerd by aluminum, red dots are oxygen and hydrogens are omitted.

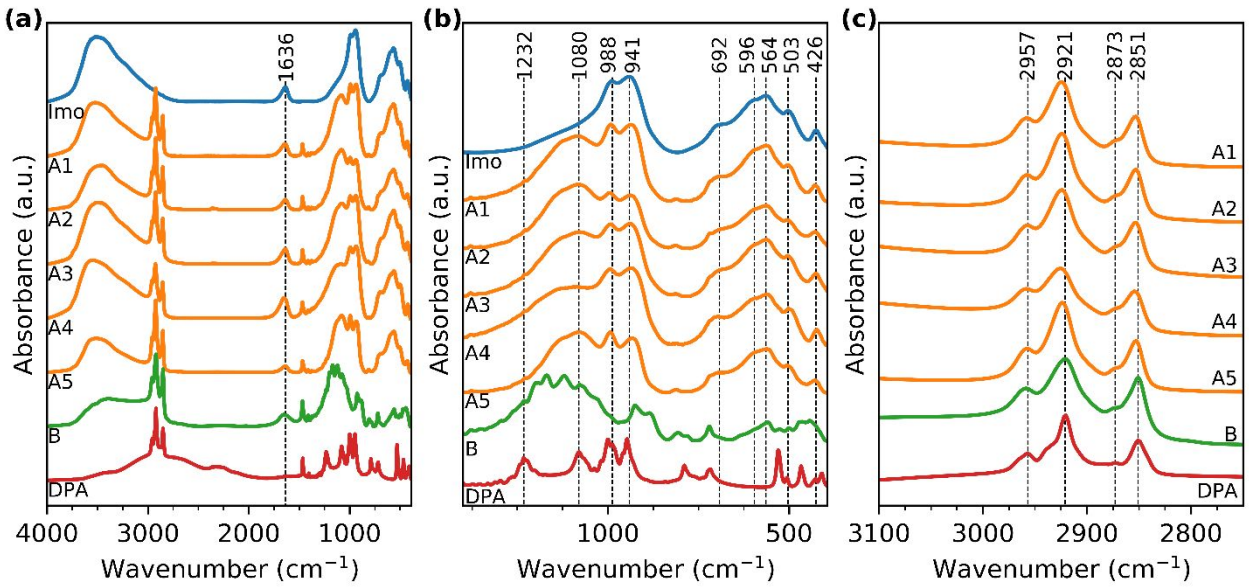

Figure 2. (a) FT-IR spectra of DPA(red), of imogolite (blue), samples A1 – A5 (orange) and sample B (green), normalized to maximum absorbance.

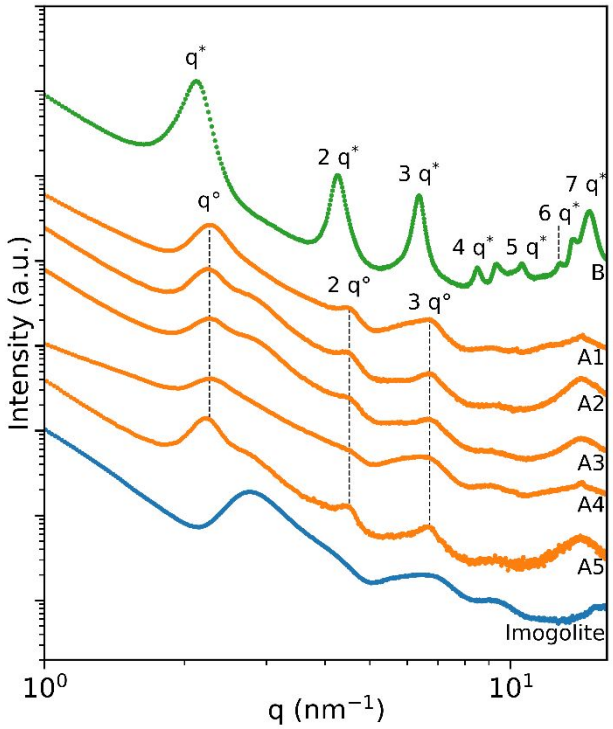

Figure 3. Powder X-ray scattering patterns of imogolite (blue), samples A1 – A5 (orange) and sample B (green).

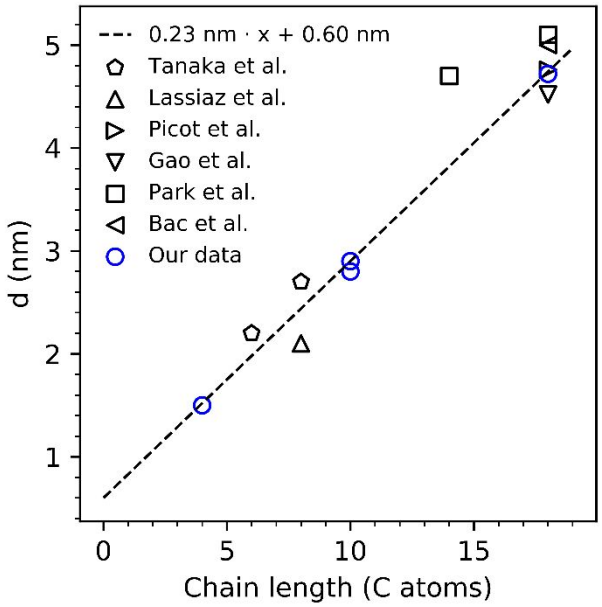

Figure 4. Repeat distance d in relation to the used alkylphosphonic acid chain length in several phosphonate phases by Tanaka et al.[42], Lassiaz et al.[25], Picot et al.[20], Gao et al.[24], Park et al.[16], Bac et al.[19] and our data. Scattering patterns and conditions for aluminum octadecyl- and butylphosphonate can be found in supplementary material (Figure S6).

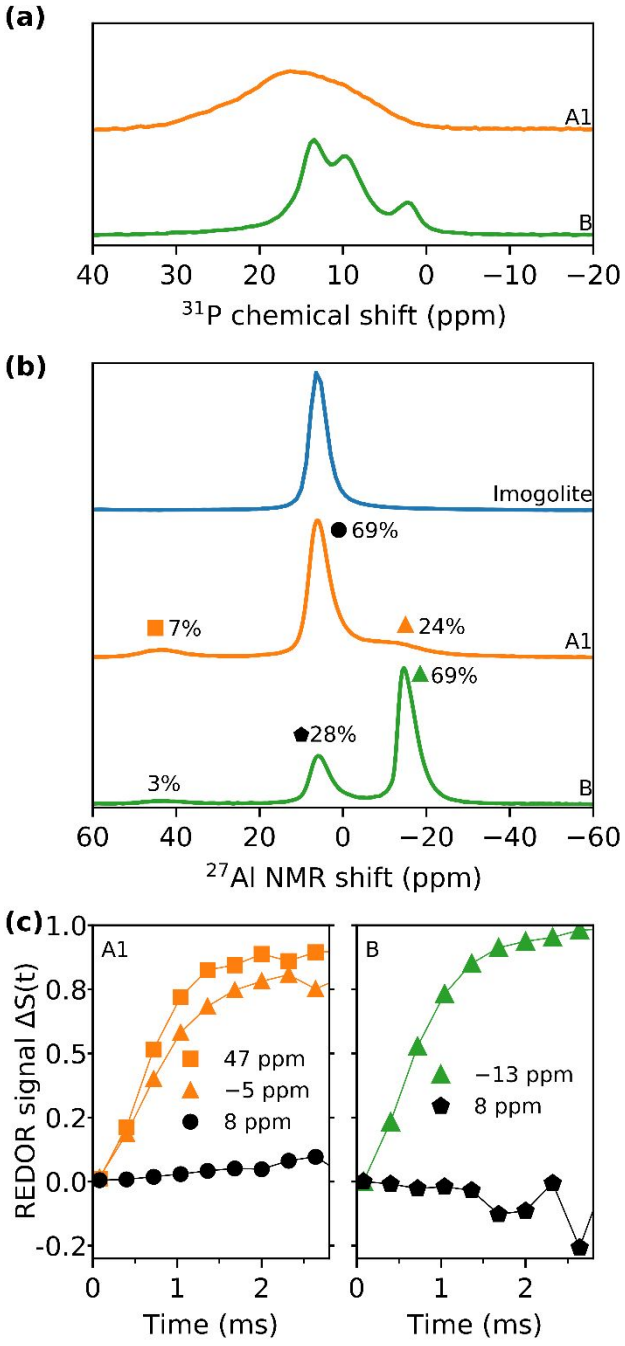

Figure 5. (a) ^{31}P MAS NMR spectra of sample A1 (orange) and sample B (green). (b) ^{27}Al MAS NMR spectra of imogolite (blue), sample A1 (orange) and sample B (green), normalized to highest peak intensity. (c) ^{27}Al {^{31}P} REDOR signals of the three sites found in sample A1 (left) and sample B (right). Lines between data points are for clarity.

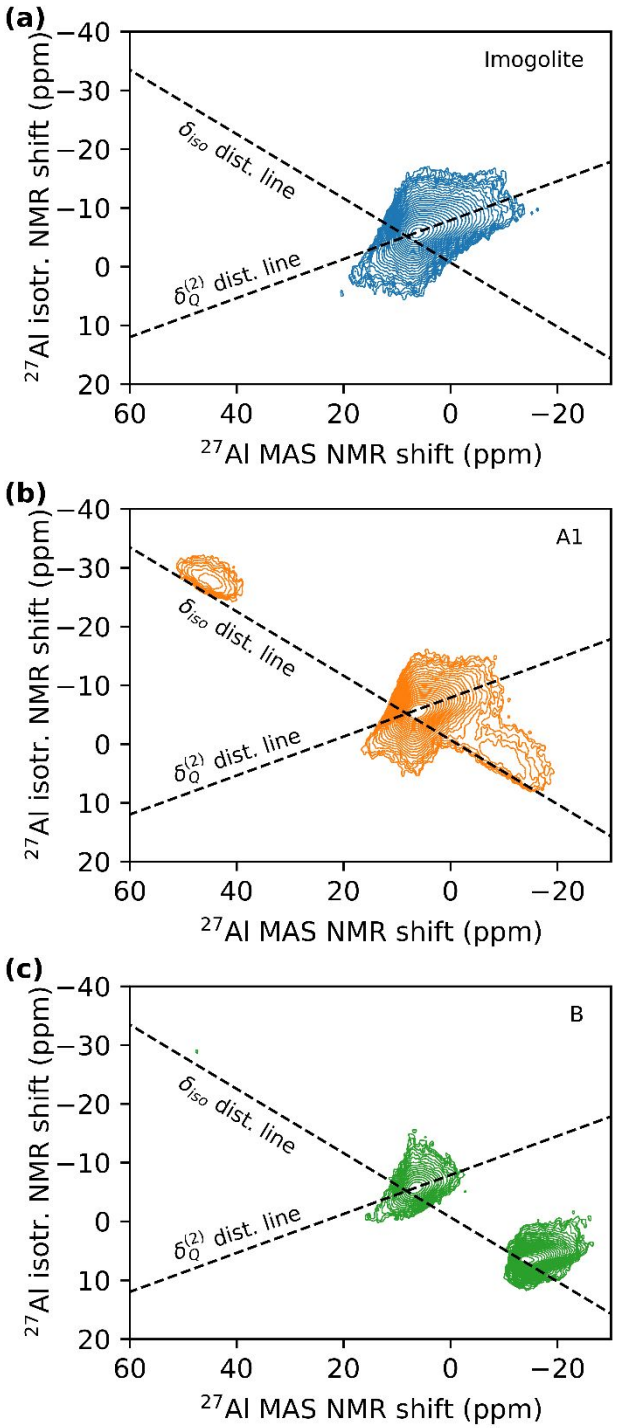

Figure 6. ^{27}Al MQMAS (triple quantum) spectra of (a) imogolite (blue), (b) sample A1 (orange) and (c) sample B (green). Dashed lines represent the directions of broadening induced by the distribution of isotropic chemical shift (δ_{iso}) and second-order quadrupolar induced shift ($\delta_Q^{(2)}$).

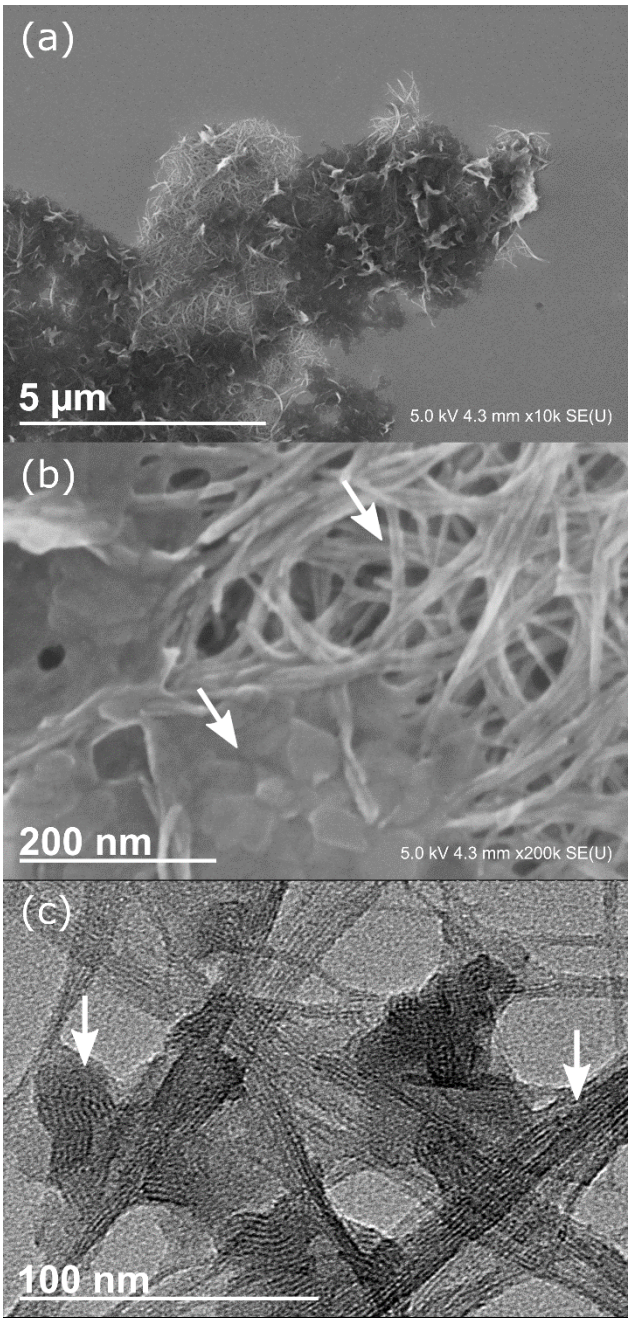

Figure 7. (a), (b) SEM picture of sample A5. (c) TEM pictures of sample A5. At least two interconnected phases are visible. Elongated bundles of aggregated imogolite and plate-like objects with a lamellar structuration.

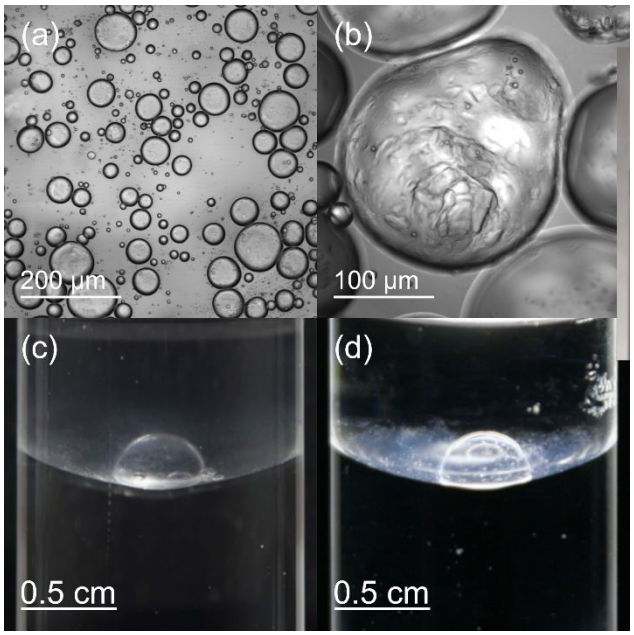

Figure 8. (a), (b) Water in oil emulsion, stabilized by sample A5 in toluene. (c) A 20 µL water droplet stabilized by modified imogolite at the toluene/water interface. (d) Stabilized droplet, illuminated from below.

References

1. Kango, S.; Kalia, S.; Celli, A.; Njuguna, J.; Habibi, Y.; Kumar, R., Surface modification of inorganic nanoparticles for development of organic–inorganic nanocomposites—A review. *Prog. Polym. Sci.* **2013,** *38* (8), 1232-1261.
2. Xavier, J.; Vincent, S.; Meder, F.; Vollmer, F., Advances in optoplasmonic sensors – combining optical nano/microcavities and photonic crystals with plasmonic nanostructures and nanoparticles. *Nanophotonics* **2018,** *7* (1), 1-38.
3. Avvakumova, S.; Colombo, M.; Tortora, P.; Prosperi, D., Biotechnological approaches toward nanoparticle biofunctionalization. *Trends Biotechnol.* **2014,** *32* (1), 11-20.
4. Guerrero, G.; Mutin, P. H.; Vioux, A., Organically modified aluminas by grafting and sol-gel processes involving phosphonate derivatives. *J. Mater. Chem.* **2001,** *11* (12), 3161-3165.
5. Thill, A., Characterisation of Imogolite by Microscopic and Spectroscopic Methods. In *Developments in Clay Science*, Elsevier: 2016; Vol. 7, pp 223-253.
6. Cradwick, P. D. G.; Farmer, V. C.; Russell, J. D.; Masson, C. R.; Wada, K.; Yoshinaga, N., Imogolite, a Hydrated Aluminium Silicate of Tubular Structure. *Nature Physical Science* **1972,** *240* (104), 187-189.
7. Miura, S.; Teramoto, N.; Shibata, M., Nanocomposites composed of poly(epsilon-caprolactone) and oligocaprolactone-modified imogolite utilizing biomimetic chelating method. *J. Polym. Res.* **2016,** *23* (2), 19.
8. Ma, W.; Kim, J.; Otsuka, H.; Takahara, A., Surface Modification of Individual Imogolite Nanotubes with Alkyl Phosphate from an Aqueous Solution. *Chem. Lett.* **2011,** *40* (2), 159-161.
9. Ma, W.; Otsuka, H.; Takahara, A., Preparation and properties of PVC/PMMA-g-imogolite nanohybrid via surface-initiated radical polymerization. *Polymer* **2011,** *52* (24), 5543-5550.
10. Ma, W.; Otsuka, H.; Takahara, A., Poly(methyl methacrylate) grafted imogolite nanotubes prepared through surface-initiated ARGET ATRP. *Chem. Commun.* **2011,** *47* (20), 5813-5815.
11. Yamamoto, K.; Otsuka, H.; Wada, S. I.; Sohn, D.; Takahara, A., Preparation and properties of [poly(methyl methacrylate)/imogolite] hybrid via surface modification using phosphoric acid ester. *Polymer* **2005,** *46* (26), 12386-12392.
12. Qi, X.; Yoon, H.; Lee, S. H.; Yoon, J.; Kim, S. J., Surface-modified imogolite by 3-APS-OsO_4 complex: Synthesis, characterization and its application in the dihydroxylation of olefins. *J. Ind. Eng. Chem.* **2008,** *14* (1), 136-141.
13. Lee, Y.; Kim, B.; Yi, W.; Takahara, A.; Sohn, D., Conducting properties of polypyrrole coated imogolite. *Bull. Korean Chem. Soc.* **2006,** *27* (11), 1815-1818.
14. Yamamoto, K.; Otsuka, H.; Takahara, A.; Wada, S. I., Preparation of a novel (polymer/inorganic nanofiber) composite through surface modification of natural aluminosilicate nanofiber. *J. Adhes.* **2002,** *78* (7), 591-602.
15. Yamamoto, K.; Otsuka, H.; Wada, S.; Takahara, A., Surface modification of aluminosilicate nanofiber "imogolite". *Chem. Lett.* **2001,** (11), 1162-1163.
16. Park, S.; Lee, Y.; Kim, B.; Lee, J.; Jeong, Y.; Noh, J.; Takahara, A.; Sohn, D., Two-dimensional alignment of imogolite on a solid surface. *Chem. Commun.* **2007,** (28), 2917-2919.
17. Yah, W. O.; Irie, A.; Otsuka, H.; Sasaki, S.; Yagi, N.; Sato, M.; Koganezawa, T.; Takahara, A., Molecular Aggregation States of Imogolite/P3HT Nanofiber Hybrid. *J. Phys.: Conf. Ser.* **2011,** *272* (1), 012021.
18. Yah, W. O.; Irie, A.; Jiravanichanun, N.; Otsuka, H.; Takahara, A., Molecular Aggregation State and Electrical Properties of Terthiophenes/Imogolite Nanohybrids. *Bull. Chem. Soc. Jpn.* **2011,** *84* (9), 893-902.
19. Bac, B. H.; Song, Y.; Kim, M. H.; Lee, Y. B.; Kang, I. M., Surface-modified aluminogermanate nanotube by OPA: Synthesis and characterization. *Inorg. Chem. Commun.* **2009,** *12* (10), 1045-1048.

20. Picot, P.; Tache, O.; Malloggi, F.; Coradin, T.; Thill, A., Behaviour of hybrid inside/out Janus nanotubes at an oil/water interface. A route to self-assembled nanofluidics? *Faraday Discuss.* **2016,** *191*, 391-406.
21. Li, M.; Brant, J. A., Dispersing surface-modified imogolite nanotubes in polar and non-polar solvents. *J. Nanopart. Res.* **2018,** *20* (2), 19.
22. Li, M.; Brant, J. A., Synthesis of polyamide thin-film nanocomposite membranes using surface modified imogolite nanotubes. *J. Membr. Sci.* **2018,** *563*, 664-675.
23. Gardolinski, J. E. F. C.; Lagaly, G.; Czank, M., On the destruction of kaolinite and gibbsite by phenylphosphonic, phenylphosphinic and phenylarsonic acids: evidence for the formation of new Al compounds. *Clay Miner.* **2004,** *39* (04), 391-404.
24. Gao, W.; Dickinson, L.; Grozinger, C.; Morin, F. G.; Reven, L., Self-assembled monolayers of alkylphosphonic acids on metal oxides. *Langmuir* **1996,** *12* (26), 6429-6435.
25. Lassiaz, S.; Galarneau, A.; Trens, P.; Labarre, D.; Mutin, H.; Brunel, D., Organo-lined alumina surface from covalent attachment of alkylphosphonate chains in aqueous solution. *New J. Chem.* **2010,** *34* (7), 1424-1435.
26. Farmer, V. C.; Fraser, A. R.; Tait, J. M., Synthesis of imogolite: a tubular aluminium silicate polymer. *J. Chem. Soc., Chem. Commun.* **1977,** (13), 462-463.
27. Lindner, P.; Zemb, T., *Neutrons, X-rays and Light: Scattering Methods Applied to Soft Condensed Matter* 1st ed.; Elsevier Science B. V.: Amsterdam, 2002.
28. Massiot, D.; Touzo, B.; Trumeau, D.; Coutures, J. P.; Virlet, J.; Florian, P.; Grandinetti, P. J., Two-dimensional magic-angle spinning isotropic reconstruction sequences for quadrupolar nuclei. *Solid State Nucl. Magn. Reson.* **1996,** *6* (1), 73-83.
29. Fyfe, C. A.; Mueller, K. T.; Grondey, H.; Wongmoon, K. C., Solid-State Double-Resonance Nmr Experiments Involving Quadrupolar and Spin 1/2 Nuclei. *J. Phys. Chem.* **1993,** *97* (51), 13484-13495.
30. Angeli, F.; Charpentier, T.; de Ligny, D.; Cailleteauz, C., Boron Speciation in Soda-Lime Borosilicate Glasses Containing Zirconium. *J. Am. Ceram. Soc.* **2010,** *93* (9), 2693-2704.
31. Du, P.; Yuan, P.; Thill, A.; Annabi-Bergaya, F.; Liu, D.; Wang, S., Insights into the formation mechanism of imogolite from a full-range observation of its sol-gel growth. *Appl. Clay Sci.* **2017,** *150*, 115-124.
32. Amara, M. S.; Paineau, E.; Rouzière, S.; Guiose, B.; Krapf, M.-E. M.; Taché, O.; Launois, P.; Thill, A., Hybrid, Tunable-Diameter, Metal Oxide Nanotubes for Trapping of Organic Molecules. *Chem. Mater.* **2015,** *27* (5), 1488-1494.
33. Picot, P.; Liao, Y. Y.; Barruet, E.; Gobeaux, F.; Coradin, T.; Thill, A., Exploring hybrid imogolite nanotubes formation via Si/Al stoichiometry control. *Langmuir* **2018,** *34* (44), 13225-13234.
34. Liao, Y.; Picot, P.; Brubach, J.-B.; Roy, P.; Le Caër, S.; Thill, A., Self-supporting thin films of imogolite and imogolite-like nanotubes for infrared spectroscopy. *Appl. Clay Sci.* **2017,** *164*, 58-67.
35. Wilson, M. A.; Lee, G. S. H.; Taylor, R. C., Tetrahedral rehydration during imogolite formation. *J. Non-Cryst. Solids* **2001,** *296* (3), 172-181.
36. Creton, B.; Bougeard, D.; Smirnov, K. S.; Guilment, J.; Poncelet, O., Molecular Dynamics Study of Hydrated Imogolite. 1. Vibrational Dynamics of the Nanotube. *J Phys Chem C* **2008,** *112* (27), 10013-10020.
37. Lee, H.; Jeon, Y.; Lee, Y.; Lee, S. U.; Takahara, A.; Sohn, D., Thermodynamic Control of Diameter-Modulated Aluminosilicate Nanotubes. *J Phys Chem C* **2014,** *118* (15), 8148-8152.
38. Peng, L.; Yu, J.; Li, J.; Li, Y.; Xu, R., Lamellar Mesostructured Aluminophosphates: Intercalation of n-Alkylamines into Layered Aluminophosphate by Ultrasonic Method. *Chem. Mater.* **2005,** *17* (8), 2101-2107.

39. Szillies, S.; Thissen, P.; Tabatabai, D.; Feil, F.; Fürbeth, W.; Fink, N.; Grundmeier, G., Formation and stability of organic acid monolayers on magnesium alloy AZ31: The role of alkyl chain length and head group chemistry. *Appl. Surf. Sci.* **2013,** *283*, 339-347.
40. Yah, W. O.; Takahara, A.; Lvov, Y. M., Selective modification of halloysite lumen with octadecylphosphonic acid: new inorganic tubular micelle. *J. Am. Chem. Soc.* **2012,** *134* (3), 1853-1859.
41. Chaplais, G.; Le Bideau, J.; Leclercq, D.; Mutin, H.; Vioux, A., Novel aluminium phenyl, benzyl, and bromobenzylphosphonates: structural characterisation and hydration-dehydration reactions. *J. Mater. Chem.* **2000,** *10* (7), 1593-1601.
42. Tanaka, H.; Chikazawa, M., Modification of amorphous aluminum phosphate with alkyl phosphates. *Mater. Res. Bull.* **2000,** *35* (1), 75-84.
43. Tanaka, H.; Watanabe, T.; Chikazawa, M.; Kazuhiko, K.; Ishikawa, T., Formation and structure of calcium alkyl phosphates. *Colloids Surf., A* **1998,** *139* (3), 341-349.
44. Tanaka, H.; Yasukawa, A.; Kandori, K.; Ishikawa, T., Modification of Calcium Hydroxyapatite Using Alkyl Phosphates. *Langmuir* **1997,** *13* (4), 821-826.
45. Cabeza, A.; Aranda, M. A.; Bruque, S.; Poojary, D. M.; Clearfield, A.; Sanz, J., Aluminum Phenylphosphonates: A Fertile Family of Compounds. *Inorg. Chem.* **1998,** *37* (17), 4168-4178.
46. Barron, P. F.; Wilson, M. A.; Campbell, A. S.; Frost, R. L., Detection of imogolite in soils using solid state 29Si NMR. *Nature* **1982,** *299* (5884), 616-618.
47. Yucelen, G. I.; Choudhury, R. P.; Vyalikh, A.; Scheler, U.; Beckham, H. W.; Nair, S., Formation of single-walled aluminosilicate nanotubes from molecular precursors and curved nanoscale intermediates. *J. Am. Chem. Soc.* **2011,** *133* (14), 5397-412.
48. Zanzottera, C.; Vicente, A.; Celasco, E.; Fernandez, C.; Garrone, E.; Bonelli, B., Physico-Chemical Properties of Imogolite Nanotubes Functionalized on Both External and Internal Surfaces. *J Phys Chem C* **2012,** *116* (13), 7499-7506.
49. Müller, D.; Gessner, W.; Samoson, A.; Lippmaa, E.; Scheler, G., Solid-state aluminium-27 nuclear magnetic resonance chemical shift and quadrupole coupling data for condensed AlO4tetrahedra. *J. Chem. Soc., Dalton Trans.* **1986,** (6), 1277-1281.
50. Haky, J. E.; Brady, J. B.; Dando, N.; Weaver, D., Synthesis and structural studies of layered aluminum phenylphosphonate. *Mater. Res. Bull.* **1997,** *32* (3), 297-303.
51. Lassiaz, S.; Labarre, D.; Galarneau, A.; Brunel, D.; Mutin, P. H., Modification of silica by an organic monolayer in aqueous medium using octylphosphonic acid and aluminium species. *J. Mater. Chem.* **2011,** *21* (22), 8199-8205.
52. Parfitt, R. L.; Fraser, A. R.; Russell, J. D.; Farmer, V. C., ADSORPTION ON HYDROUS OXIDES: II. OXALATE, BENZOATE AND PHOSPHATE ON GIBBSITE. *J. Soil Sci.* **1977,** *28* (1), 40-47.
53. McBride, M. B.; Wesselink, L. G., Chemisorption of catechol on gibbsite, boehmite, and noncrystalline alumina surfaces. *Environ. Sci. Technol.* **1988,** *22* (6), 703-708.
54. Van Emmerik, T. J.; Sandstrom, D. E.; Antzutkin, O. N.; Angove, M. J.; Johnson, B. B., 31P solid-state nuclear magnetic resonance study of the sorption of phosphate onto gibbsite and kaolinite. *Langmuir* **2007,** *23* (6), 3205-13.
55. Luengo, C. V.; Castellani, N. J.; Ferullo, R. M., Quantum chemical study on surface complex structures of phosphate on gibbsite. *Spectrochim. Acta, Part A* **2015,** *147*, 193-199.
56. Cao, G.; Hong, H. G.; Mallouk, T. E., Layered metal phosphates and phosphonates: from crystals to monolayers. *Acc. Chem. Res.* **1992,** *25* (9), 420-427.
57. Laiti, E.; Persson, P.; Ohman, L. O., Balance between surface complexation and surface phase transformation at the alumina/water interface. *Langmuir* **1998,** *14* (4), 825-831.
58. Abe, H.; Matsue, T.; Yabu, H., Reversible Shape Transformation of Ultrathin Polydopamine-Stabilized Droplet. *Langmuir* **2017,** *33* (25), 6404-6409.
59. Aussillous, P.; Quéré, D., Liquid marbles. *Nature* **2001,** *411* (6840), 924-927.

60. Liu, Y.; Zhang, X.; Poyraz, S.; Zhang, C.; Xin, J. H., One-Step Synthesis of Multifunctional Zinc-Iron-Oxide Hybrid Carbon Nanowires by Chemical Fusion for Supercapacitors and Interfacial Water Marbles. *ChemNanoMat* **2018,** *4* (6), 546-556.